Stable synchronised states of coupled Tchebyscheff maps

C. P. Dettmann*

November 11, 2002

Abstract

Coupled Tchebyscheff maps have recently been introduced to explain parameters in the standard model of particle physics, using the stochastic quantisation of Parisi and Wu. This paper studies dynamical properties of these maps, finding analytic expressions for a number of periodic states and determining their linear stability. Numerical evidence is given for nonlinear stability of some of these states, and also the presence of exponentially slow dynamics for some ranges of the parameter. These results indicate that a theory of particle physics based on coupled map lattices must specify strong physical arguments for any choice of initial conditions, and explain how stochastic quantisation is obtained in the many stable parameter regions.

1 Introduction

Coupled map lattices [1] consist of a continuous variable (here Φ) defined on a discrete lattice representing space and time. The dynamics relates the value of Φ at each space-time point to its value at previous lattice points, typically just the most recent time and the nearest neighbours in space. Coupled map lattices include the simplest examples of spatiotemporal chaos and are often used to model less tractable systems such as nonlinear partial differential equations.

Diffusively coupled Tchebyscheff maps were introduced by Beck in order to chaotically quantise field theories [2], later applied to spontaneous symmetry breaking of quantised Higgs fields [3]. The discrete time of the coupled map lattice corresponds to the fictitious time in the Parisi-Wu stochastic quantisation [4], and is taken to infinity in order to reproduce quantum mechanics. The function appearing in the map is naturally given by the derivative of the quartic double well potential, which (appropriately scaled) is the third degree Tchebyscheff polynomial discussed below. In addition, Tchebyscheff maps

*Department of Mathematics, University of Bristol, University Walk Bristol BS8 1TW, UK

are conjugated to Bernoulli shifts, and so have very chaotic statistical properties, hence the possibility that the stochastic forces arise intrinsically from the chaotic dynamics.

In a later work [5], Beck considers coupled map lattices based on the second degree Tchebyscheff polynomial in addition to the third degree case considered previously, and restricts attention to one spatial dimension. He numerically computes averages of interaction and self energies, and reproduces to about four digits a large number of parameters occurring in the standard model of particle physics, with predictions for some poorly constrained quantities such as neutrino and Higgs masses.

The opinion of the present author is that although Ref. [5] does not contain a complete theory relating particle physics to coupled map lattices, the probability of obtaining such a large number of accurate predictions with so few adjustable parameters is sufficiently small that the models warrant further attention.

Quite apart from the context in which these models were introduced, they have a number of appealing features from a dynamical point of view. In particular, there is an adjustable parameter a in which the system takes two exactly solvable limits, $a = 0$ which is decoupled and fully chaotic, and $a = 1$ in which the lattice decouples into two sub-lattices, the latter of which are fully chaotic for the advanced coupling case and fully stable for the backward coupling case (see below for definitions).

Motivated by the desire for exact results and the simple form of the equations, this paper analyses the simplest periodic states, those for which the field does not depend on the spatial variable, called "synchronised states". Finding these states is equivalent to finding periodic orbits of a one dimensional map, but the linear stability is a more involved calculation than one dimensional maps due to spatially dependent unstable modes. Stability analysis is important because the proliferation of stable states undermines the argument that stochastic quantisation arises from the chaotic dynamics.

A general theory of linear stability of periodic solutions of coupled map lattices is given in Refs. [6, 7]. Our analysis of synchronised states leads, as in these works, to cyclic matrices, which are always explicitly diagonalisable. The general theory also permits spatially periodic solutions of length greater than one (leading to block cyclic matrices), and lattices of spatial dimension greater than one (leading to blocks within blocks).

Finding that an orbit in a spatially extended system is linearly stable does not imply that a finite measure of initial conditions approaches the orbit, unlike finite dimensional dynamical systems. Actually, there are many possible inequivalent measures of initial conditions: we choose an initial distribution that is Lebesgue in the field Φ and spatially independent, but physical arguments may justify an alternative choice. In fact, in view of the results, we will argue that the final (ie infinite fictitious time) state depends strongly on this choice of initial conditions, and hence that physical arguments are required to specify such a choice.

The linear stability of the synchronised states is given in Sec. 2. Numerical work in Sec. 3 reveals properties of the dynamics far from these periodic states. The conclusion summarises the results, discussing in more detail the implications for the Beck theory.

Model	f	g
$2A$	$T_2(\Phi)$	$T_2(\Phi)$
$2A^-$	$T_2(\Phi)$	$-T_2(\Phi)$
$2B$	$T_2(\Phi)$	Φ
$2B^-$	$T_2(\Phi)$	$-\Phi$
$3A$	$T_3(\Phi)$	$T_3(\Phi)$
$3B$	$T_3(\Phi)$	Φ

Table 1: Definitions of functions f and g appearing in Eq. (1) for the coupled map lattices considered in this paper. The Tchebyscheff polynomials are $T_N(\Phi) = \cos(N \arccos \Phi)$, specifically $T_2(\Phi) = 2\Phi^2 - 1$ and $T_3(\Phi) = 4\Phi^3 - 3\Phi$.

2 Linear stability

2.1 Formalism

As in low dimensional dynamical systems (such as the individual maps), linear stability analysis in coupled map lattices consists of determining whether and how fast infinitesimal perturbations of a reference trajectory (here a periodic orbit) grow with time. As noted above, however, linear stability, in that *all* sufficiently small (everywhere) perturbations decay with time, does not imply that a finite measure of initial conditions is attracted to the reference trajectory. Notwithstanding ths caveats of interpretation, the linear stability analysis is a good starting point for finding stable orbits and their corresponding parameter ranges; nonlinear stability is discussed in Sec. 3.

Consider a diffusively coupled map lattice, in which x and t are integer space and time variables respectively (a more transparent notation than the conventional i and n respectively):

$$\Phi_{x,t+1} = (1-a)f(\Phi_{x,t}) + \frac{a}{2}\left[g(\Phi_{x+1,t}) + g(\Phi_{x-1,t})\right] \tag{1}$$

Here, f is the map at each site x, g couples neighboring maps with a strength a. Later we will specify f and g to be the possibilities enumerated in Tab. 1. We demand that $\Phi \in [-1, 1]$; this property is preserved if f and g are closed on this interval, and $a \in [0, 1]$. Any periodic orbits found by solving the appropriate equations are only relevant if they lie in this range.

Synchronised states are solutions in which $\Phi_{x,t}$ is independent of x, and so are given by the one dimensional map

$$\Phi_{t+1} = (1-a)f(\Phi_t) + ag(\Phi_t) \tag{2}$$

which is a weighted mean of the f and g maps. To a first approximation, stable solutions of the full coupled map lattice which are periodic in time occur when the synchronised map (2) has a superstable periodic orbit, that is, when one of its critical points is mapped back to itself after some time, leading to a Lyapunov exponent of $-\infty$. We will observe that the linear stability properties of the full coupled map lattice are slightly different from that of the synchronised map, so that although stability occurs in the region of synchronised superstable orbits, the superstable orbit may not be linearly stable in the extended system.

The difference between stability in the synchronised map and the extended system is that the full coupled map lattice has an infinite number of degrees of freedom, leading to a richer spectrum of possible instabilities. Differentiating Eq. (1) leads to the evolution of the perturbations

$$\delta\Phi_{x,t+1} = (1-a)f'(\Phi_t)\delta\Phi_{x,t} + \frac{a}{2}\left[g'(\Phi_t)\delta\Phi_{x-1,t} + g'(\Phi_t)\delta\Phi_{x+1,t}\right] \tag{3}$$

or in matrix form

$$\delta\Phi_{t+1} = J_t\delta\Phi_t \tag{4}$$

where J_t is a cyclic (assuming periodic boundary conditions) tridiagonal matrix,

$$J_t = \begin{pmatrix} (1-a)f'(\Phi_t) & \frac{a}{2}g'(\Phi_t) & & & \frac{a}{2}g'(\Phi_t) \\ \frac{a}{2}g'(\Phi_t) & (1-a)f'(\Phi_t) & \frac{a}{2}g'(\Phi_t) & & \\ & \frac{a}{2}g'(\Phi_t) & (1-a)f'(\Phi_t) & \frac{a}{2}g'(\Phi_t) & \\ & & & \ddots & \\ \frac{a}{2}g'(\Phi_t) & & & \frac{a}{2}g'(\Phi_t) & (1-a)f'(\Phi_t) \end{pmatrix} \tag{5}$$

The full stability matrix for a periodic orbit of (temporal) length τ is a product of the form

$$J = J_{\tau-1}J_{\tau-2}\cdots J_0 \tag{6}$$

For a cyclic matrix $M_{i,j} = m_{i-j}$ of size X (the full extent of the system in the spacelike direction), there are X eigenvectors v_k, given by

$$v_k = (1, e^{\mathrm{i}k}, e^{\mathrm{i}2k}, \ldots, e^{-\mathrm{i}k}) \tag{7}$$

where $k = 2\pi j/X$, $j = 0, 1, \ldots, X-1$. This, together with the fact that the corresponding eigenvalues λ_k are

$$\lambda_k = \sum_{j=0}^{X-1} m_j e^{\mathrm{i}jk} \tag{8}$$

follows by substitution into $Mv_k = \lambda_k v_k$.

The product of cyclic matrices J given by (6) acting on v_k thus gives $\lambda_k v_k$ where the eigenvalue is

$$\lambda_k = \prod_{t=0}^{\tau-1}\left[(1-a)f'(\Phi_t) + ag'(\Phi_t)\cos k\right] \tag{9}$$

Linear stability follows if $|\lambda_k| < 1$ for all values of k. Note that this is a stronger condition than stability of the synchronised map (2), which is $|\lambda_k| < 1$ for $k = 0$.

There are two classes of analytic results obtained using Eq. (9), $\tau \leq 2$ in which case the periodic orbits can be given exactly, and certain families of periodic orbits which are given exactly in the limit $\tau \to \infty$. These are investigated in sections 2.2 and 2.3 respectively.

Dynamics	Φ	Domain of validity	Domain of stability
$2A$	-1/2	[0,1]	None
$2A$	1	[0,1]	None
$2A^-$	$\frac{1-\sqrt{9-32a+32a^2}}{4-8a}$	[0,1]	$(\frac{5}{14} \approx 0.3571, \frac{9}{14} \approx 0.6429)$
$2B$	-1/2	[0,1]	None
$2B$	1	[0,1]	None
$2B^-$	$\frac{1+a-\sqrt{9-14a+9a^2}}{4-4a}$	[0,1]	$(\frac{5}{9} \approx 0.5556, 1)$
$3A$	-1	[0,1]	None
$3A$	0	[0,1]	None
$3A$	1	[0,1]	None
$3B$	-1	[0,1]	None
$3B$	0	[0,1]	None
$3B$	1	[0,1]	None

Table 2: Synchronised states of period $\tau = 1$. The first column gives the model as defined in Tab. 1. The second column gives the solution of Eqs. (2,10). The third column gives values of a for which $\Phi \in [0, 1]$. The fourth column gives values of a for which $|\lambda_k| < 1 \forall k$ in Eq. (9), that is, the orbits are linearly stable.

2.2 Synchronised states of periods one and two

The equation for the synchronised dynamics (2) leads directly to states of period τ by imposing the condition

$$\Phi_{t+\tau} = \Phi_t \tag{10}$$

For $\tau = 2$ it might be supposed that such an equation may have very complicated, possibly non-closed form solutions, since for the cubic maps the relevant polynomial is of degree 9 (albeit reducible to degree 6 by noting that the fixed point $\tau = 1$ solutions can be removed). It turns out that, even in this case, the solution can be written using arithmetic operations together with at most two square-root operations.

The periodic orbits are given in Tables 2, 3. We start by noting that maps $2A$ and $3A$, for which the synchronised maps (2) are just the original Tchebyscheff maps, have no stable periodic orbits as these are fully expanding when transformed to the variable $\phi = \arccos \Phi$. The fixed points ($\tau = 1$) of the $2B$ and $3B$ maps are similar in that they are always unstable, and in that the solution Φ does not depend on a. The remaining periodic orbits for $\tau \leq 2$ have regions of stability in a.

The calculations here are quite straightforward, so details will be given for only the most complicated case, the $\tau = 2$ orbits of the $3B$ model. The solutions of the equations (2, 10) are obtained using a symbolic manipulation package, and are given in Tab. 3 and plotted in Fig. 1, where the three orbits are designated “central”, “upper” and “lower”. Equation (9) reads

$$\lambda_k = [3(1-a)(4\Phi_+^2 - 1) + a \cos k][3(1-a)(4\Phi_-^2 - 1) + a \cos k] \tag{11}$$

Dynamics	Φ	Domain of validity	Domain of stability
$2A$	$\frac{-1\pm\sqrt{5}}{4}$	[0,1]	None
$2A^{-}$	$\frac{-1\pm\sqrt{5-32a+32a^2}}{4-8a}$	$[0,\frac{4-\sqrt{6}}{8}\approx 0.1938]$	$(\frac{7-2\sqrt{7}}{14}\approx 0.1220, 1/6\approx 0.1667)$
		$[\frac{4+\sqrt{6}}{8}\approx 0.8062, 1]$	$(5/6\approx 0.8333, \frac{7+2\sqrt{7}}{14}\approx 0.8780)$
$2B$	$\frac{-1-a\pm\sqrt{5-18a+9a^2}}{4-4a}$	$[0, 1/3\approx 0.3333]$	$(\frac{3-\sqrt{6}}{3}\approx 0.1835, \frac{11-\sqrt{96}}{5}\approx 0.2404)$
$2B^{-}$	$\frac{-1+a\pm\sqrt{5-14a+9a^2}}{4a-4}$	$[0, 5/9\approx 0.5556]$	$(\frac{5-\sqrt{10}}{5}\approx 0.3675, 5/9\approx 0.5556)$
$3A$	$\pm\frac{\sqrt{2}}{2}$	[0,1]	None
$3A$	$\frac{1\pm\sqrt{5}}{4}$	[0,1]	None
$3A$	$-\frac{1\pm\sqrt{5}}{4}$	[0,1]	None
$3B$	$\pm\sqrt{\frac{1-2a}{2-2a}}$	$[0, 1/2 = 0.5000]$	$(1/4 = 0.2500, 2/5 = 0.4000)$
$3B$	$\pm\sqrt{\frac{3-4a\pm\sqrt{5-24a+16a^2}}{8-8a}}$	$([0, 1/4 = 0.2500]$	$[\frac{21-\sqrt{281}}{20}\approx 0.2118, 1/4 = 0.2500)$
$3B$	$\pm\sqrt{\frac{3-4a\mp\sqrt{5-24a+16a^2}}{8-8a}}$	$[0, 1/4 = 0.2500]$	$(\frac{21-\sqrt{281}}{20}\approx 0.2118, 1/4 = 0.2500)$

Table 3: Synchronised states of period $\tau = 2$. Columns as in Tab. 2 except that the two values of Φ are represented by the $\pm$ signs. The $2A^{-}$ model has two disjoint domains of validity of the given orbit.

where

$$4\Phi_{\pm}^2 - 1 = \begin{cases} \frac{1-2a\pm\sqrt{5-24a+16a^2}}{2-2a} & \text{upper} \\ \\ \frac{1-3a}{1-a} & \text{central} \\ \\ \frac{1-2a\mp\sqrt{5-24a+16a^2}}{2-2a} & \text{lower} \end{cases} \tag{12}$$

The maximum value of λ_k is determined from

$$0 = \frac{d\lambda_k}{dk} = -a\sin k[3(1-a)(4\Phi_{+}^2 - 1 + 4\Phi_{-}^2 - 1) + 2a\cos k] \tag{13}$$

for which possible solutions are $k = 0$, $k = \pi$, and

$$\cos k = -\frac{3(1-a)(4\Phi_{+}^2 - 1 + 4\Phi_{-}^2 - 1)}{2a} = \begin{cases} -3\frac{1-2a}{2a} & \text{upper/lower} \\ \\ -3\frac{1-3a}{a} & \text{central} \end{cases} \tag{14}$$

These solutions can be substituted back into Eq. (11) taking care to exclude ranges of a in which $\cos k$ is not in $[-1, 1]$.

For the central orbit, the $k = 0$ solution gives

$$\lambda_k = 9 - 48a + 64a^2 \tag{15}$$

which has magnitude greater than one for $a < 1/4$. The $k = \pi$ solution gives

$$\lambda_k = 9 - 60a + 100a^2 \tag{16}$$

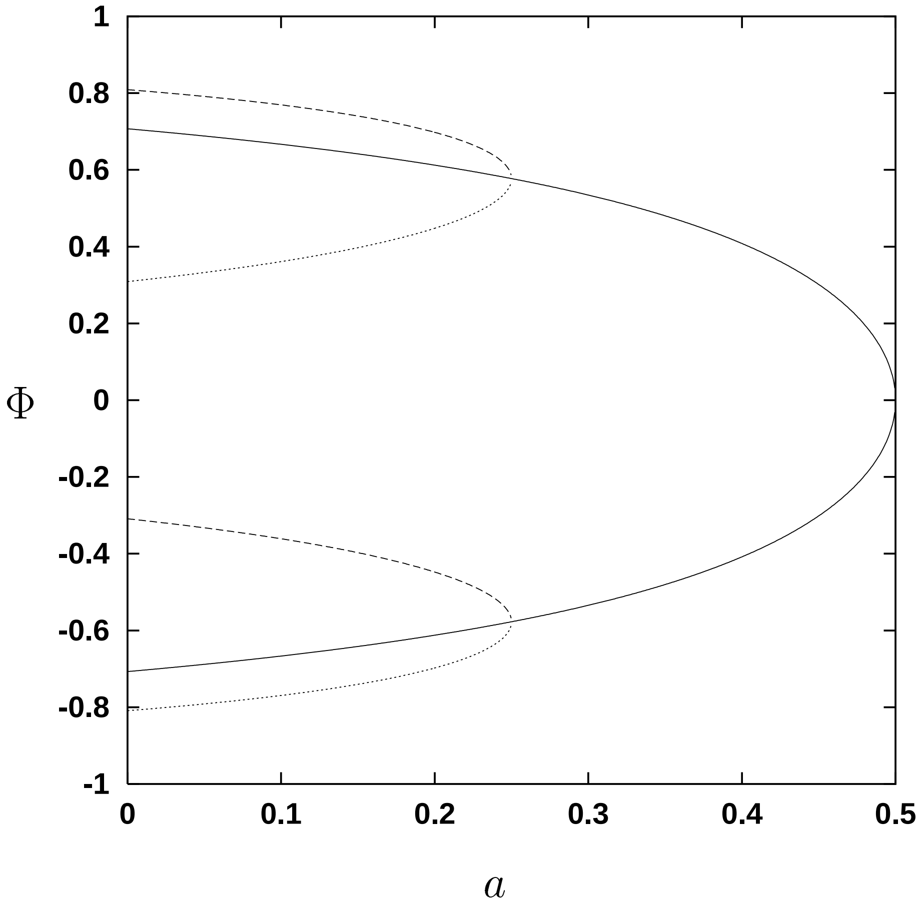

Figure 1: Period 2 orbits of the $3B$ model. The three orbits (see Tab. 3) are shown using solid, dashed and dotted lines for the "central", "upper" and "lower" orbits respectively; in each case there are two values of Φ.

which has magnitude greater than one for $a < 1/5$ and $a > 2/5$. The solution $\cos k = -3(1-3a)/a$ is in the range $[-1, 1]$ for $a > 3/10$ and gives

$$\lambda_k = 0 \tag{17}$$

Thus the domain of linear stability for the central orbit is $(1/4, 2/5)$ as given in Tab. 3.

For the upper and lower orbits, the $k = 0$ solution gives

$$\lambda_k = -9 + 48a - 32a^2 \tag{18}$$

which has magnitude greater than one for $a < (3-\sqrt{5})/4 \approx 0.1910$. It is also equal to one at the maximum value of a for the orbits, $a = 1/4$. The $k = \pi$ solution gives

$$\lambda_k = -9 + 42a - 20a^2 \tag{19}$$

which has magnitude greater than one for $a < (21-\sqrt{281})/20 \approx 0.2118$. The other solution $\cos k = -3(1-2a)/(2a)$ is never in the range $[-1, 1]$ for $a \leq 1/4$, and so is irrelevant. Thus the domain of linear stability for the upper and lower orbits is $((21-\sqrt{281})/20, 1/4)$ as given in Tab. 3. The linear stability for all orbits is presented in Fig. 2.

In this manner all the other domains of linear stability in Tables 2 and 3 were generated. Apart from the $2A$ and $3A$ models for which the synchronised dynamics is unaffected by the coupling, there are analytically tractable linearly stable domains of period 2 for all models. Among the interesting features are the bifurcation observed in the $3B$ model (see Fig. 1), and two regions of stability in the $2A_-$ model (see Tab. 3). We now move to the other analytically tractable case, the limit $\tau \to \infty$.

2.3 Synchronised states of long period

This section gives an analytic treatment of families of synchronised stable orbits with long period. The idea is similar to that of the superstable orbits of (for example) the logistic map, in which the critical point (at which the derivative is zero) maps back to itself after a number of iterations, leading to a periodic orbit with a Lyapunov exponent of $-\infty$. Here the extended nature of the dynamics complicates and destabilises the dynamics to a degree, however linear stability is still possible, as we shall show.

In the original Tchebyscheff maps the critical points are pre-images of unstable fixed points at $\Phi = \pm 1$, and so never return to form a superstable orbit. However, the synchronised map (2) is, for small a, and excluding the $2A$ and $3A$ cases, a small perturbation on the Tchebyscheff map, so that after a "long" time (of order $-\ln a$) the trajectory can return to the critical point. There are many possible ways in which this can happen; we focus here on the simplest in which the trajectory, after at most a single point near $\Phi = -1$ always remains in the rightmost branch of the map. An example of such a periodic orbit is given in Fig. 3.

We now locate a periodic orbit of length τ, and in particular calculate the value of a at which it is close to superstable. Suppose that for some value of a, the initial point is close to the critical point, that is,

$$\Phi_0 = \mathcal{O}(a) \tag{20}$$

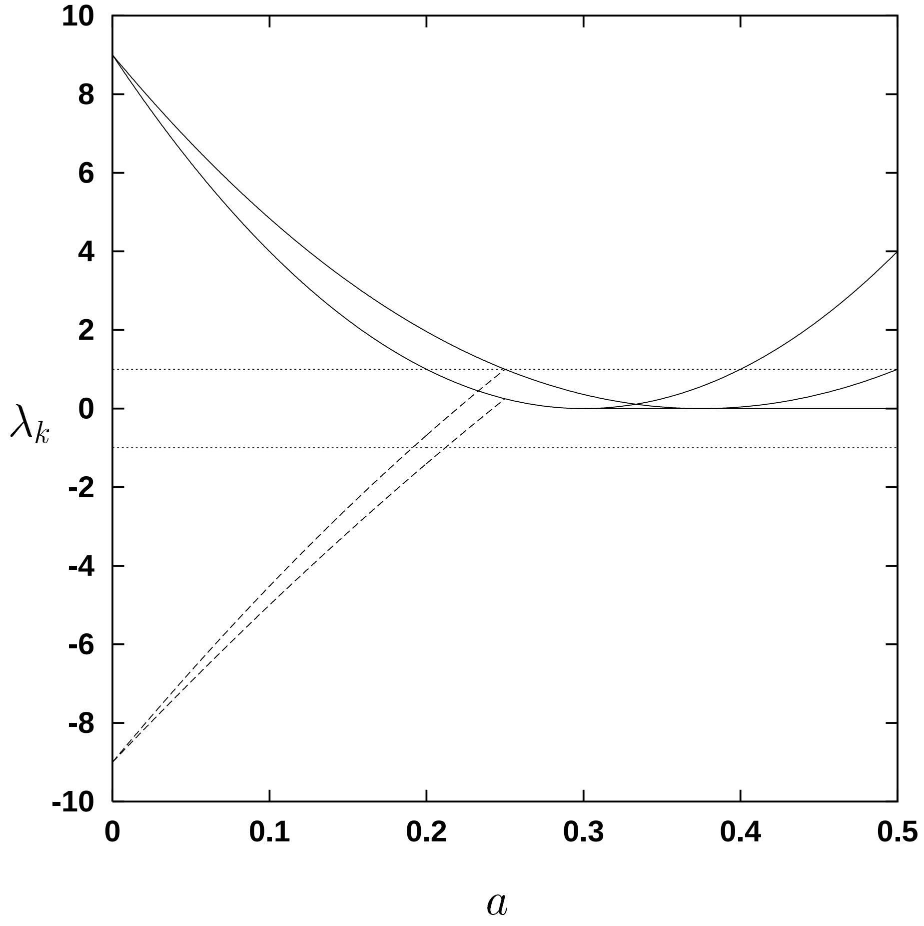

Figure 2: Linear stability of the orbits shown in Fig. 1. Depending on the value of k, λ_k takes values between the solid or dashed lines for the central or other orbits respectively. The orbits are linearly stable if all λ_k for a given orbit lie between the dotted lines. Formulas for these lines are in Eqs. (15-19).

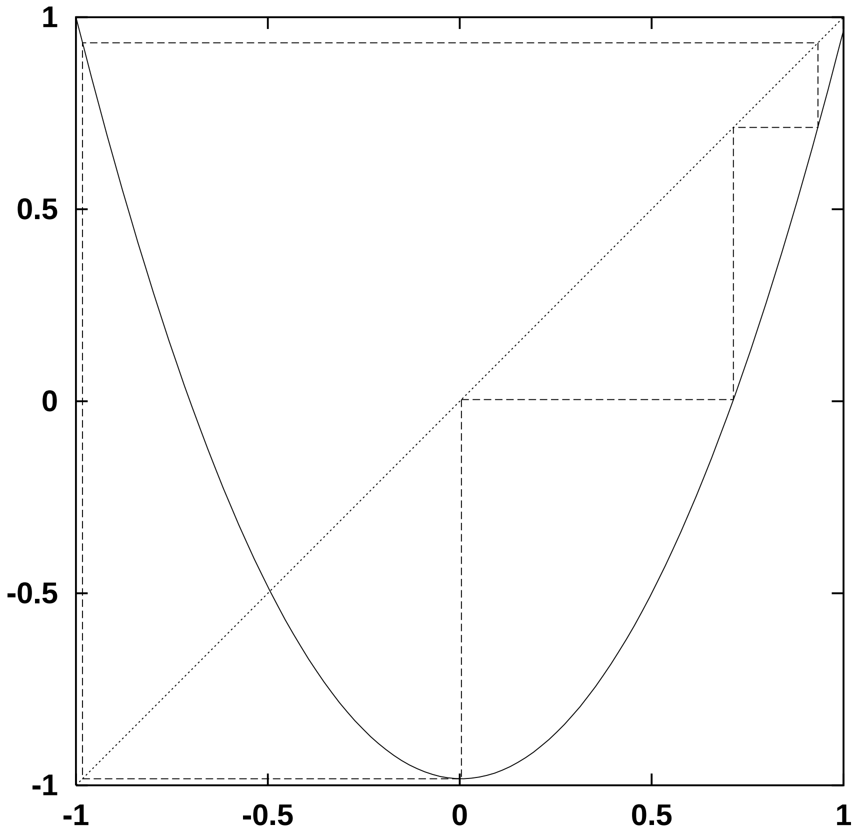

Figure 3: Stable $\tau = 4$ orbit of the $2B^{-}$ synchronised map, Eq. (2). In this case $a = 0.0171$, slightly greater than the value $a^{*}/N^{\tau} = 0.0165$ predicted by the large τ theory (see Tab. 4 below).

Model	b_1	b_2	d	b^*	a^*	π^*	λ^*
$2A_-$	2	10	2	2/3	$3\pi^2/16 \approx 1.851$	$1/(2\pi)$	0
$2B$	1	6	0	3/8	$\pi^2/3 \approx 3.290$	$1/(2\pi)$	$\pi/6 \approx 0.5236$
$2B_-$	1	4	2	7/24	$3\pi^2/7 \approx 4.230$	$1/(2\pi)$	$3\pi/14 \approx 0.6732$
$3B$	3/2	27/2	0	1/6	$4\pi^2/3 \approx 13.159$	$1/(4\pi\sqrt{3})$	$\pi/(3\sqrt{3}) \approx 0.6046$

Table 4: Coefficients of the long period orbits, defined throughout Sec. 2.3.

for the second degree maps (that is, $2A^-$, $2B$ and $2B^-$) and

$$\Phi_0 = -1/2 + \mathcal{O}(a) \tag{21}$$

for the third degree map $3B$. We can use Eq. (2) to find the successive iterates. We have

$$\Phi_1 = -1 + b_1 a + \mathcal{O}(a^2) \tag{22}$$

for the second degree maps and

$$\Phi_1 = 1 - b_1 a + \mathcal{O}(a^2) \tag{23}$$

for the third degree map. Here b_1 is a known constant that depends on the map, and is given in Tab. 4. Iterating again, we have

$$\Phi_2 = 1 - b_2 a + \mathcal{O}(a^2) \tag{24}$$

for all maps. Again, b_2 is given in Tab. 4 for each model.

Further iterates remain near the unstable fixed point of the unperturbed map at $\Phi = 1$, that is, we have

$$\Phi_j = 1 - b_j a + \mathcal{O}(a^2) \tag{25}$$

where each successive b_j is obtained from the previous one by an equation of the form

$$b_{j+1} = N^2 b_j + d \tag{26}$$

where N is the degree of the map (two or three) and d is given in Tab. 4 for each map. The recursion (26) is a linear difference equation, solved by multiplying through by $N^{-2(j+1)}$ and summing over j from 2 to $m-1$. The result is

$$b_n = N^{2(m-2)} b_2 + d\frac{N^{2(m-2)} - 1}{N^2 - 1} \approx N^{2m} b^* \tag{27}$$

where

$$b^* = \frac{b_2}{N^4} + \frac{d}{N^6 - N^4} \tag{28}$$

is also given in Tab. 4.

As the trajectory approaches the end of the periodic orbit, Φ deviates substantially from 1, invalidating the above approximation. This part of the trajectory is obtained by iterating $\Phi_0 = \Phi_\tau$ backwards. Recalling that the Tchebyscheff polynomials can be represented as $T_n(\Phi) = \cos n \arccos \Phi$ we have for the degree 2 models

$$\Phi_{\tau-1} = \cos\frac{\pi}{4} + \mathcal{O}(a) = \sqrt{\frac{1}{2}} + \mathcal{O}(a) \tag{29}$$

$$\Phi_{\tau-2} = \cos\frac{\pi}{8} + \mathcal{O}(a) = \sqrt{\frac{1}{2}\left(1+\sqrt{\frac{1}{2}}\right)} + \mathcal{O}(a) \tag{30}$$

$$\Phi_{\tau-n} = \cos\frac{\pi}{2^{n+1}} + \mathcal{O}(4^{-n}a) = \sqrt{\frac{1}{2}\left(1+\sqrt{\frac{1}{2}\,(1+\ldots)}\right)} + \mathcal{O}(4^{-n}a) \tag{31}$$

and for the degree 3 model

$$\Phi_{\tau-n} = \cos\frac{2\pi}{3^{n+1}} + \mathcal{O}(9^{-n}a) \tag{32}$$

Note that the $\mathcal{O}(a)$ corrections are suppressed by the contraction of the inverse map.

The orbit is closed by matching the expressions for Φ_m and $\Phi_{\tau-n}$, assuming that both m and n (actually N^{2m} and N^{2n}) are much greater than one. The result is

$$1 - b^* 4^{\tau-n} a + \mathcal{O}(4^{-n}a) = 1 - \frac{1}{2}\left(\frac{\pi}{2^{n+1}}\right)^2 + \mathcal{O}(4^{-2n}) \tag{33}$$

for the second degree models and

$$1 - b^* 9^{\tau-n} a + \mathcal{O}(9^{-n}a) = 1 - \frac{1}{2}\left(\frac{2\pi}{3^{n+1}}\right)^2 + \mathcal{O}(9^{-2n}) \tag{34}$$

for the third degree model. The value of a can now be read off as

$$a = a^* N^{-2\tau} + \mathcal{O}(N^{-4\tau}) \tag{35}$$

where a^* is given in Tab. 4. The result is consistent with the original assumption that a is small. Note that the original $\mathcal{O}(a)$ freedom in the initial condition Φ_0 contributes to $\mathcal{O}(a^2)$ when the trajectory is near $\Phi = 1$, and so is expected to shift a by an amount of order a^2, that is, $N^{-4\tau}$. Obtaining the appropriate coefficient would require a more involved calculation.

Now we turn to the linear stability of these long orbits using Eq. (9). λ_k is now a product of a large number (τ) of factors. The $t = 0$ factor is small since both $f'(\Phi_0)$ and a are small, and will be considered separately. For the remaining factors the $f'(\Phi)$ term dominates and the $g'(\Phi)$ term can be ignored, owing to the presence of the small quantity a. Thus we have

$$\lambda_k = [f'(\Phi_0) + a g'(\Phi_0)\cos k] \prod_{t=1}^{\tau-1} f'(\Phi_t)[1 + \mathcal{O}(a\tau)] \tag{36}$$

The product is

$$\prod_{t=1}^{\tau-1} f'(\Phi_t) = -\prod_{t=1}^{\tau-1} 4\cos\frac{\pi}{2^{\tau-t+1}} = -\prod_{t=1}^{\tau-1} 2\frac{\sin\frac{\pi}{2^{\tau-t}}}{\sin\frac{\pi}{2^{\tau-t+1}}} = -2^{\tau-1}\frac{\sin\frac{\pi}{2}}{\sin\frac{\pi}{2^\tau}} \tag{37}$$

for the second degree models, ignoring corrections of order a. An analogous result holds for the third degree model. Making a small angle approximation we arrive at

$$\left|\prod_{t=1}^{\tau-1} f'(\Phi_t)\right| = N^{2\tau}\pi^* \tag{38}$$

where π^* is given in Tab. 4. Thus the product, being of order $N^{2\tau}$, balances the first factor which is of order a and hence $N^{-2\tau}$. An orbit will be linearly stable if the remaining coefficient maximised over k (and denoted λ^*) is less than one.

We can set $f'(\Phi_0) = 0$ by letting $\Phi_0 = 0$ for the second degree models and $\Phi_0 = -1/2$ for the $3B$ model. For the $2A^-$ model we also have $g'(0) = 0$ so the orbit remains superstable in the presence of perturbations at all wavenumbers k, and $\lambda^* = 0$. The B models have $g'(0) = \pm 1$, so that we have stability if $\lambda^* = a^*\pi^* < 1$. This quantity is also given in Tab. 4, and it shows that all orbits are linearly stable when $f'(\Phi_0) = 0$.

Note that the most stable state is when $f'(\Phi) = 0$ belongs to a periodic orbit of the synchronised map (2); this is not generally the same as the superstable point of this map, which is the solution of the equation $(1-a)f'(\Phi) + ag'(\Phi) = 0$.

Finally we make a connection to an observation made in Ref. [5]. In section 6.6 of that work a scaling was observed numerically in the limit $a \to 0$, in particular the dynamical average

$$V(\Phi) = \langle \int_0^\Phi f(\Phi')d\Phi' \rangle \tag{39}$$

exhibited the following behaviour

$$V(a) - V(0) = h(a)\sqrt{a} \tag{40}$$

where the function $h(a)$ satisfies (in the limit)

$$h(N^2 a) = h(a) \tag{41}$$

that is, $h(a)$ is log-periodic. Here we have found a family of stable orbits in which a differs from one to the next by a factor of N^2. The N^2 comes from the derivative of the synchronised map at the points $\Phi = \pm 1$. The scaling of N^2 would occur in other families of orbits (stable or unstable) containing $\Phi = \pm 1$, and hence possibly to all small values of a.

3 Nonlinear stability

Linear stability, considered in the previous section, implies that sufficiently small perturbations of a periodic state will approach that state in the future. However, this does not imply that a generic initial state will approach the stable state. For a sufficiently large system, some of the initial conditions will be near points of the periodic state, however there is no guarantee that neighbouring maps will not strongly perturb these maps away from the periodic state.

This section contains numerical results that use an initial state in which the $\Phi_{x,0}$ initial conditions are independently distributed uniformly from the interval $[-1, 1]$. The spatial size of the system is 10^3 maps with periodic boundary conditions. After a time of 10^4 units the values of Φ for each of the maps are plotted for many values of the parameter a. The results do not depend noticeably on the spatial extent, but do depend on the relaxation time (see below). See Fig. 4.

The boundaries of the linearly stable orbits of period 1 and 2 given in Tabs. 2 and 3 are shown as vertical lines; most of these boundaries are clearly bifurcations. The period 1 orbits are both stable; the period 2 orbits while having a clearly observable effect on the dynamics, do not appear to be the entire attractor; the high period orbits discussed in Sec. 2.3 appear completely absent, although they are visible if the initial conditions are chosen closer to the periodic state.

The most interesting question is what has happened to the period 2 orbits. Looking at the $2B^-$ in figure 4, the period 2 orbit bounds a discrete set of values for $0.3675 < a < 0.48$ and a continuous set of values for $0.48 < a < 0.5556$. In both cases a spatial slice of the solution reveals intermittent switching between the two values, as shown in Fig. 5. The discrete case contains dynamically "frozen" domains which remain for all time. The continuous case relaxes by increasing the size of the domains, but does so exponentially slowly.

In the discrete case, there is no relaxation, so the final state (and consequently any property of it, such as the average V in Eq, (39) depends strongly on the choice of initial conditions; a different distribution function for the initial conditions would lead to a different distribution of domains. Averages can be estimated given a knowledge of the relative proportions of upper domains, lower domains and boundary regions. Other properties such as spatial correlation functions require more information about the distribution of domains.

The continuous case is numerically ambiguous due to the exponentially long time scales. It may may relax eventually to the stable periodic orbit, so its infinite time properties can be calculated directly from this orbit.

As the relaxation time increases, the transition between the discrete and continuous regimes (ie $a = 0.48$ at a time of 10^4) is observed to move towards larger a, so it is in fact likely that at sufficiently long times, the final destination is a state with frozen disorder for all a corresponding to this stable periodic orbit. For example, the lower right plot in Fig. 5 shows that at $a = 0.5$ and a time of 10^8 the dynamics seems to have frozen.

However, even if as suggested in Ref. [5] the coupled map lattice describes something going on at the Planck scale (10^{-35} seconds), the transient relaxation may relate to measurable time scales. Note that time in the coupled map lattice is not physical time but Parisi-Wu fictitious time which supposedly is taken to infinity. The question is

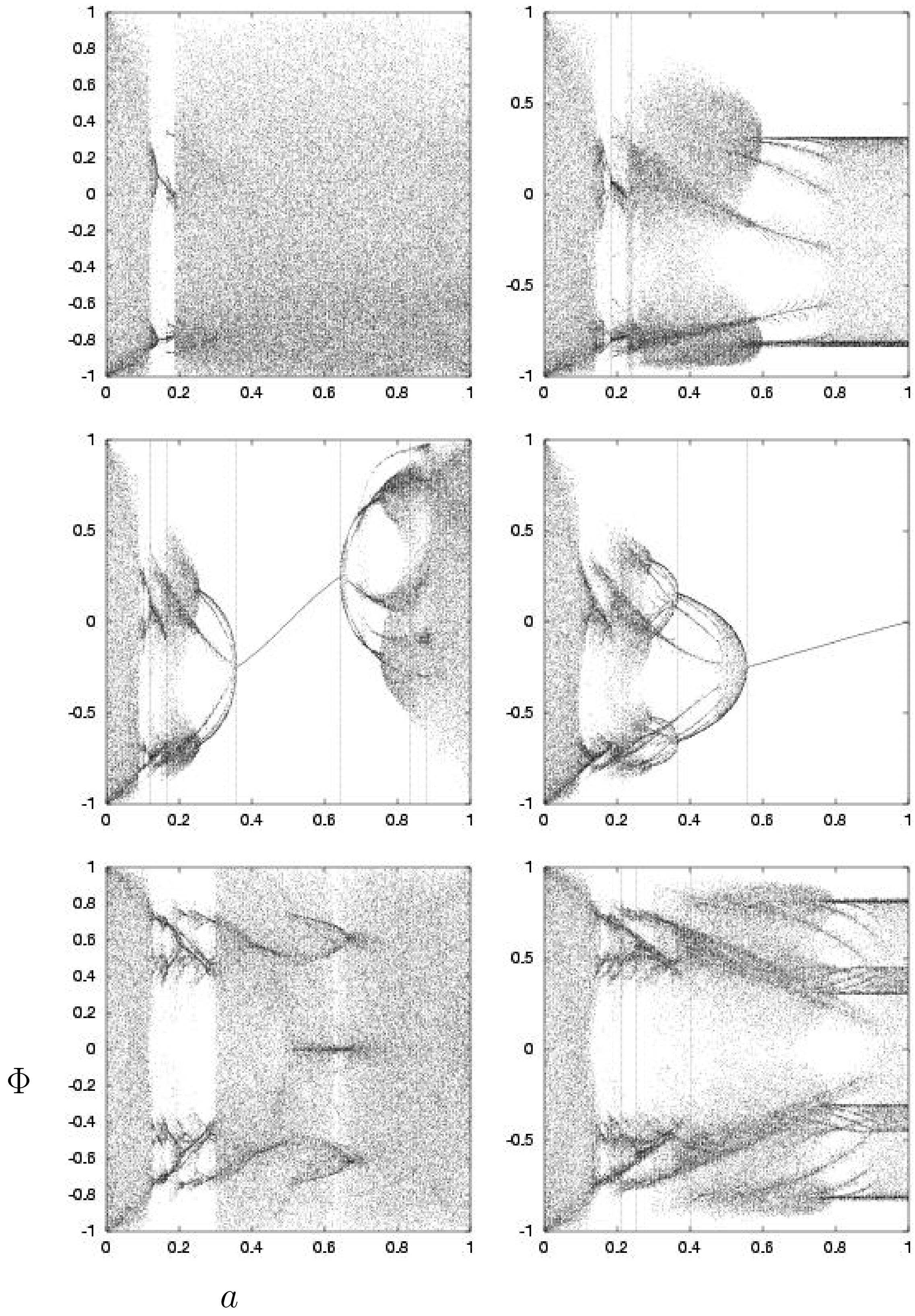

Figure 4: Bifurcation diagrams for each of the models. The left column from top are $2A$, $2A^{-}$ and $3A$ respectively; the right column is the same with A replaced by B. The vertical lines indicate boundaries of linearly stable orbits from Tabs. 2, 3.

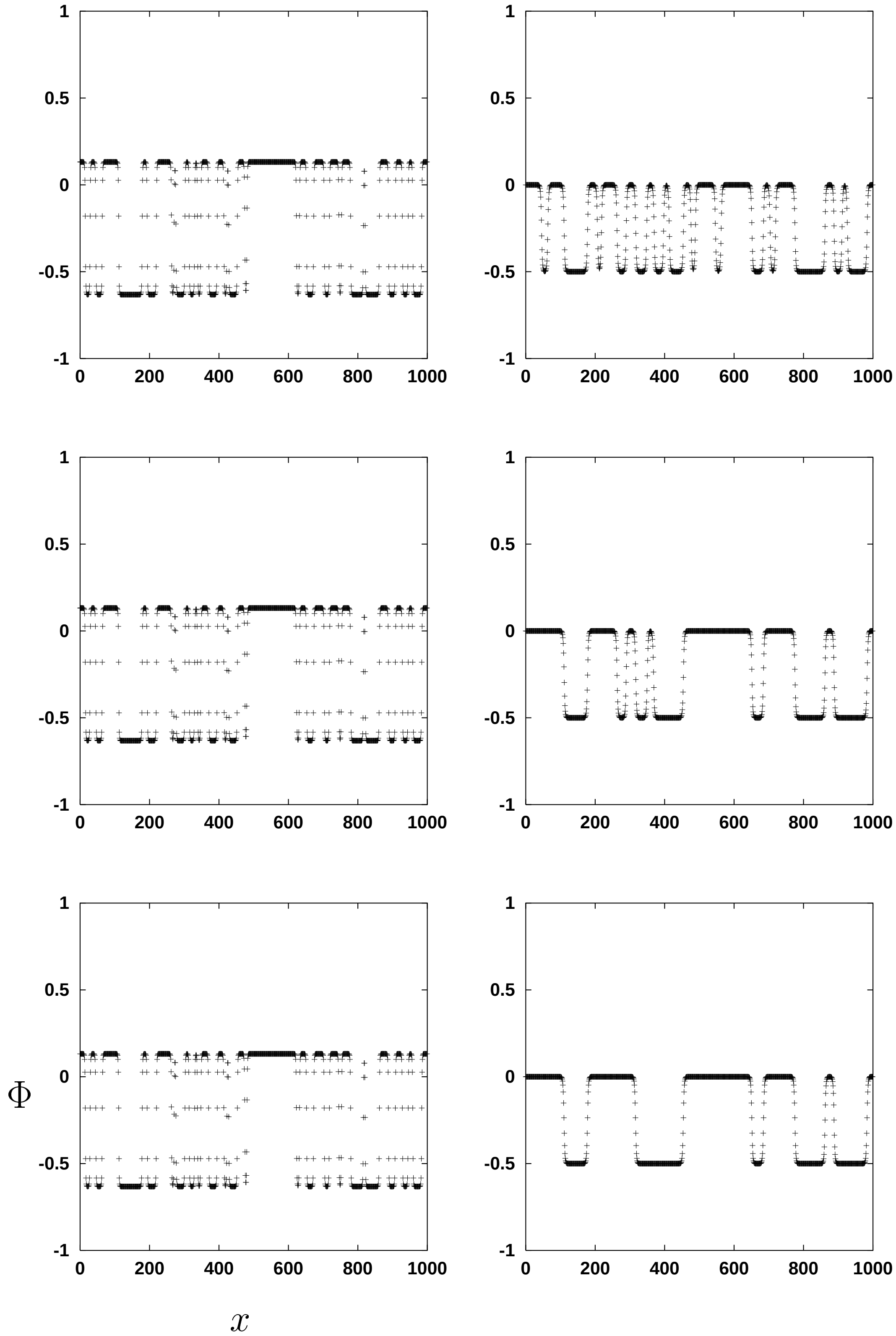

Figure 5: Spacelike slices of the period 2 orbit of the $2B_-$ map, showing frozen disorder ($a = 0.4$, left) and exponentially slow relaxation ($a = 0.5$, right). The relaxation times are 10^4 (top), 10^6 (middle) and 10^8 (bottom)

whether this indeed happens or rather it remains exponentially large but finite.

The other backward coupled (B) maps and also $2A_-$ have the same appearance of multiple "feathered" attracting points, which apparently give way to a continuous distribution as a is varied, specifically for $2B$ and $a > 0.6$, for $2A^-$ and $a \approx 0.3$ or $a \approx 0.7$, and for $3B$ and $a > 0.8$. It seems likely that this phenomenon of exponentially slow dynamics and strong dependence on initial conditions holds for all of these regimes also.

The other general feature, noted in Ref. [5], is that for small a, the advanced (A) and backward (B) coupled maps lead to very similar behaviour.

Comparing Fig. 4 here with the results in Ref. [5], the following points (from which the standard model parameters are calculated) are in regions with apparently stable attractors:

First, the interaction energy zeros: $a_3^{(3B)} \approx 0.35$ lies in the domain of stability of a period two orbit, however the numerical results suggest chaos here (for our uniformly distributed initial conditions), albeit strongly focussed on a small range of Φ. $a_1^{(2A)} \approx 0.12$ lies just below the lower boundary of the stable window (of spatial period 2; not discussed above). $a_1^{(2A^-)} \approx 0.18$ is close to the boundary of stability of the period 2 orbit at $1/6$. $a_2^{(2A^-)} = 1/2$ and $a_2^{(2B^-)} = 1$ both lie in the stable (period one) regions as noted in Ref. [5].

Second, the self energy extrema: $a'^{3A}_7 \approx 0.17$ and $a'^{3A}_8 \approx 0.23$ both lie in a complicated stable region, as do $a'^{3B}_7 \approx 0.19$ and $a'^{(3B)\approx 0.29}_8$, the latter of which is corresponds to a stable period two orbit. $a'^{(2A)}_3 \approx 0.18$ lies close to the upper boundary of the stable window mentioned in the previous paragraph. $a'^{(2B)}_3 \approx 0.22$ lies in a stable period 2 orbit, although numerical results suggest chaos in its vicinity.

Thus, these values (and hence standard model parameters according to Ref. [5]) relate to many different types of dynamics, from fully chaotic (ie not in the lists above) to a stable fixed point. Only the latter is easily obtained analytically.

4 Conclusion

Coupled Tchebyscheff maps provide excellent scope for both analytic and numerical studies of stable synchronised states. Periodic states of (temporal) length one and two can be found analytically, and are found to have linear stability for a number of models in various ranges of the parameter a. Numerical observations confirm transitions at values predicted by the theory.

There is also a family of orbits of increasing length that can be handled analytically in the long period limit, which demonstrates the existence of local stability, even arbitrarily close to the uncoupled fully chaotic limit $a = 0$.

Numerically, the period 2 orbit in the $2B^-$ model is an attractor where the two values of Φ occur in different domains at one time slice, exchanging their values at the next time slice. The size and distribution of these domains depends sensitively on the distribution of initial conditions. Furthermore, some values of a require exponentially long times before the final state is reached. Similar structures appear in the $2A^-$, $2B$ and $3B$ models.

How do these results affect Ref. [5]? In general we might expect the results to depend on the choice of initial conditions if a stable periodic state exists (true for many of the values) or indeed any coexistence of attractors (beyond the scope of this paper), and also be affected by exponentially slow dynamics in one of the "feather" regions (apparently not relevant at the values given in Ref. [5]).

In addition, the fact that many if not most of the values of a correspond to stability, or at least not full chaos, undermines the assertion that it is the strong chaotic properties of the Tchebyscheff maps that is responsible (via stochastic quantisation) for quantum mechanics. The coupled Tchebyscheff maps are often far from chaotic, and some explanation must be given as to why many stable parameter values are important in particle physics yet the quantisation mechanism requires strong instability.

The results presented here are only a brief sketch of the diffusively coupled Tchebyscheff map lattices, however it has been sufficient to find analytic results for classes of periodic states and demonstrate some of the richness of spatially extended dynamics including bifurcations evident in Figs. 1 and 4, and exponentially slow dynamics in Fig. 5. The combination of analytic tractability and a great variety of dynamical behaviour makes the coupled Tchebyscheff maps good candidates for prototypes of spatiotemporal chaos, much as the (closely related) logistic map is a prototype of low dimensional chaos.

Acknowledgements

The author thanks C. Beck and J. R. Dorfman for helpful discussions. Financial support was provided by the Nuffield Foundation, grant NAL/00353/G.

References

[1] K. Kaneko (Ed.), *Theory and applications of coupled map lattices* Wiley, New York (1993).

[2] C. Beck, Nonlinearity **8**, 423-441 (1995).

[3] C. Beck, Phys. Lett. A **248**, 386-392 (1998).

[4] G. Parisi and Y. S. Wu, Sci. Sinica **24**, 483-496 (1981).

[5] C. Beck, Physica D **171**, 72-106 (2002); *Spatiotemporal chaos and vacuum fluctuations of quantized fields* World Scientific, London (2002).

[6] R. E. Amritkar, P. M. Gade, A. D. Gangal, and V. M. Nandkumaran, Phys. Rev. A **44**, R3407-R3410 (1991).

[7] P. M. Gade and R. E. Amritkar, Phys. Rev. E **47**, 143-154 (1993).